Scientific Research Publishing

Open Journal of Earthquake Research, 2022, 11, 89-107
https://www.scirp.org/journal/ojer
ISSN Online: 2169-9631
ISSN Print: 2169-9623

High-Precision Structural Map of Southeast Cameroon Using Phase Filters on Potential Gravimetric Data

Nzeuga Alain Rodrigue[1*], Bisse Salomon Bertrant[1], Amaya Adama[2], Kenfack Fokem Alpha Baster[3], Ngah Christian Gislain Leonel[4], Ndjounguep Juscar[2], Nanfa Tefak Fatoumata Maelle[5], Ngoumou Paul Claude[6], Assembe Stéphane Patrick[7], Pokam Kengni Serge Hugues[7]

[1]Department of Petroleum Gas and Exploration, School of Geology and Mining Engineering, University of Ngaoundere, Meiganga, Cameroon
[2]Department of Geological Mapping and Geomatic, School of Geology and Mining Engineering, University of Ngaoundere, Meiganga, Cameroon
[3]Department of Mining Geology, School of Geology and Mining Engineering, University of Ngaoundere, Meiganga, Cameroon
[4]Postgraduate School of Science Technology and Geosciences, University of Yaounde I, Yaounde, Cameroon
[5]Institute of Mining and Geological Research, Ministry of Scientific Research, Yaounde, Cameroon
[6]Department of Geophysics, School of Geology and Mining Engineering, University of Ngaoundere, Meiganga, Cameroon
[7]Department of Physics, Faculty of Science, University of Bamenda, Bambili, Cameroon
Email: *alainzeuga@yahoo.fr

How to cite this paper: Rodrigue, N.A., Bertrant, B.S., Adama, A., Baster, K.F.A., Leonel, N.C.G., Juscar, N., Maelle, N.T.F., Claude, N.P., Patrick, A.S. and Hugues, P.K.S. (2022) High-Precision Structural Map of Southeast Cameroon Using Phase Filters on Potential Gravimetric Data. *Open Journal of Earthquake Research*, **11**, 89-107.
https://doi.org/10.4236/ojer.2022.114006

Received: June 12, 2022
Accepted: November 22, 2022
Published: November 25, 2022

Abstract

The south-east of Cameroon encompasses a wide variety of geological structures among which we can cite the Congo Craton (CC), the Sanaga Fault (SF), the Yaoundé Domain, the Panafrican belt, the Protozoic series and the Dja complex. The presence of all these structures justifies the great tectonic activity to which this area was subject from the rupture of Pangea to the creation of the different plates that exist today. In this work, we will bring out a high-resolution structural map of the study area by applying the qualitative analysis of the phase filters on 200,900 points of gravimetric data obtained from the combination of the XGM2016 and ETOPO1 models. Then, with these same data, we will bring out another structural map with the maxima method called Multi-Scale Horizontal Derivative of Vertical Derivative (MSHDVD) which will be compared to the first in order to show the limits of the MSHDVD method. To do this, we will first use the extension method to highlight the map of residual anomalies, then a combination of derivative, gradient and phase filters to highlight the geological structures responsible for fracturing in this area. Phase filters have the advantage that they make it possible to highlight

all the geological edges responsible for the fracturing without taking into account the depth, while the MSHDVD method highlights the existing geological contacts (edges) at depths well defined by the examiner. The structural map obtained with the MSHDVD method shows that the major structural direction in this zone is W-E while that obtained from the interpretation of the phase filters is more precise and shows that the major structural direction in this area would be N-S and this result would be in perfect agreement with the tectonics of East Cameroon.

Keywords

Gravimetry, Potential Field Data, Edge Detection, Structural Mapping, Southeast Cameroon

1. Introduction

Located in southeastern Cameroon, the study area (**Figure 1**) is between latitudes 1˚ and 5˚N and longitudes 12˚ and 17˚E. It covers an area of 246,469 km^2 and extends over three Central African countries, namely Gabon, Congo and the Central African Republic. Potential data provide information about sources inside the Earth on a different scale [1] [2]. Determining the residual gravity field amounts to enhance the signal of the total anomaly field by isolating them from the effects of ambient noise and shallow sources [3]. There are cases where quite large anomalies are hidden in the regional field and this is usually because the source is larger than the study area or is located at great depth. Variations in the mid to high frequencies of the gravity anomaly spectrum could reflect the influence of lithospheric structures with changes in density and topographic relief [4] [5] [6] [7] [8]. Thus, a regional/residual separation of the gravity field would be an essential numerical step in the interpretation of gravity data [9]. In the past, this issue has been addressed with a straightforward graphical approach [10] either by empirically selecting data points representative of a regional gravity field [11] [12] or by using various mathematical tools to obtain a regional gravity field [13] [14] [15] [16].

Despite numerous methods that have been developed and applied for this purpose, probably four methods among them are the most commonly used. The one that will be applied in this work includes the separation method that we used. This category is based on the analysis of the power spectra of gravity fields in order to differentiate between regional and residual gravity fields attributed to sources at different depths [17]. This procedure involves the application of the Fourier transform and gravity data filtering. The wavelength components can then be investigated for gravity fields, while selecting parameters for a separating regional and residual gravity field [18] [19] [20].

Several gravimetric and seismological studies have been carried out in this region, including the work of [21]-[27]. The main objectives were the determination

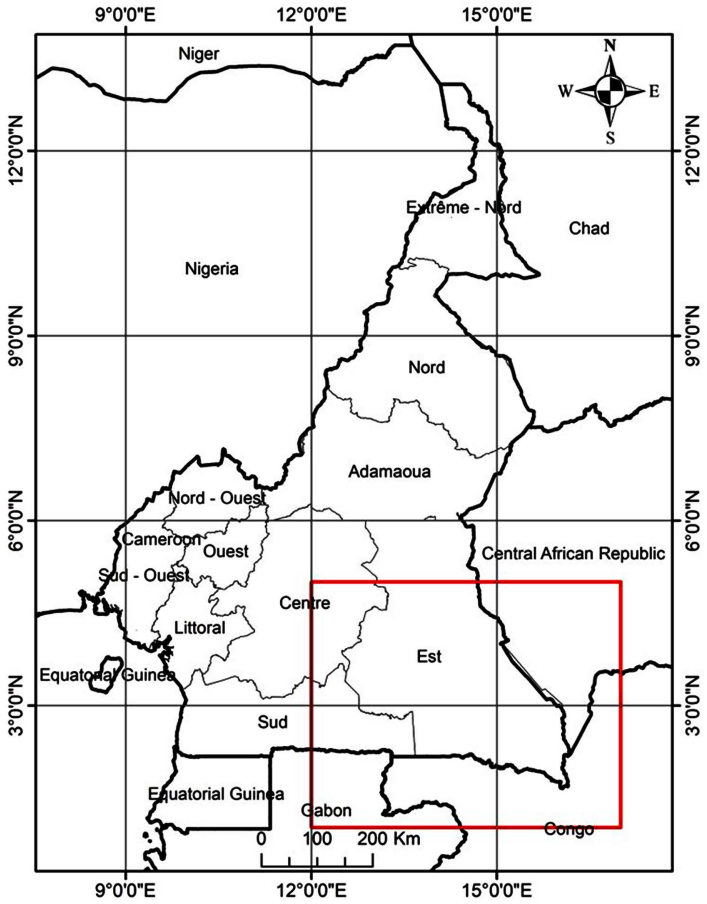

Figure 1. Location map of the study area.

of the depth of the Moho and the structural study. However, the previous structural studies were based on the method of maxima and the objective of our work for the future would be to apply the phase filters to bring out a high-resolution structural map of the south-east of Cameroon.

The use of 200,900 measurement points from the recent XGM2016 model and the regional/residual separation of the Bouguer anomaly map by the extension method could increase the signature gravity anomalies [28]. The use of the locations of the maxima method [29] and filters such as vertical derivatives, horizontal gradient amplitude [30] [31], total gradient amplitude [32] [33] [34], tilt angle [35] and horizontal gradient amplitude of tilt angle [36] can help in identification and determination of source edges and their positions.

In this work, we will use the Bouguer anomaly data to separate field components. Then we will apply the first-order derivation, the Horizontal Gradient (HG), the Analytical Signal (AS), the Tilt Angle (TDR) and the horizontal gradient of the tilt angle (HG_{TDR}) filters to highlight the different contacts. Finally, we will compare the geological contacts obtained from the combination of TDR and HG_{TDR} maps with those obtained by the multi-scale horizontal derivative of the vertical derivative method to bring out a new tectono-structural map of the region and show the limitations of the MSHDVD method.

2. Geological Setting

The geology of the southeast Cameroon as represented in Figure 2 is very complex and encompasses structures of a varied nature. It is characterised by a dentritic hydrograhic network that emphasizes a variety of tectonic features such as the Ntem complex, (a part of Congo Craton), the Yaounde domain, the Sanaga fault (SF), the Protérozoic series and the Dja complex. All these structures have already been the subject of several studies with different methods by several authors working in the field of geology. The geology of the study area could generally be divided into the Precambrian basement and Archean structure [37] [38] [39]. These two major geological features are associated with the Oubanguides Belt, formed during the Atlantic opening from the continental collision of the Archean Congo and West African Cratons in Africa together with the São Francisco Craton in South America [36] [40] [41] [42], during which NE-SW, E-W to ESE-WNW, NW-SE and N-S main lineaments were formed and the crust rejuvenated at the NW edge of the Congo Craton [43] [44] [45].

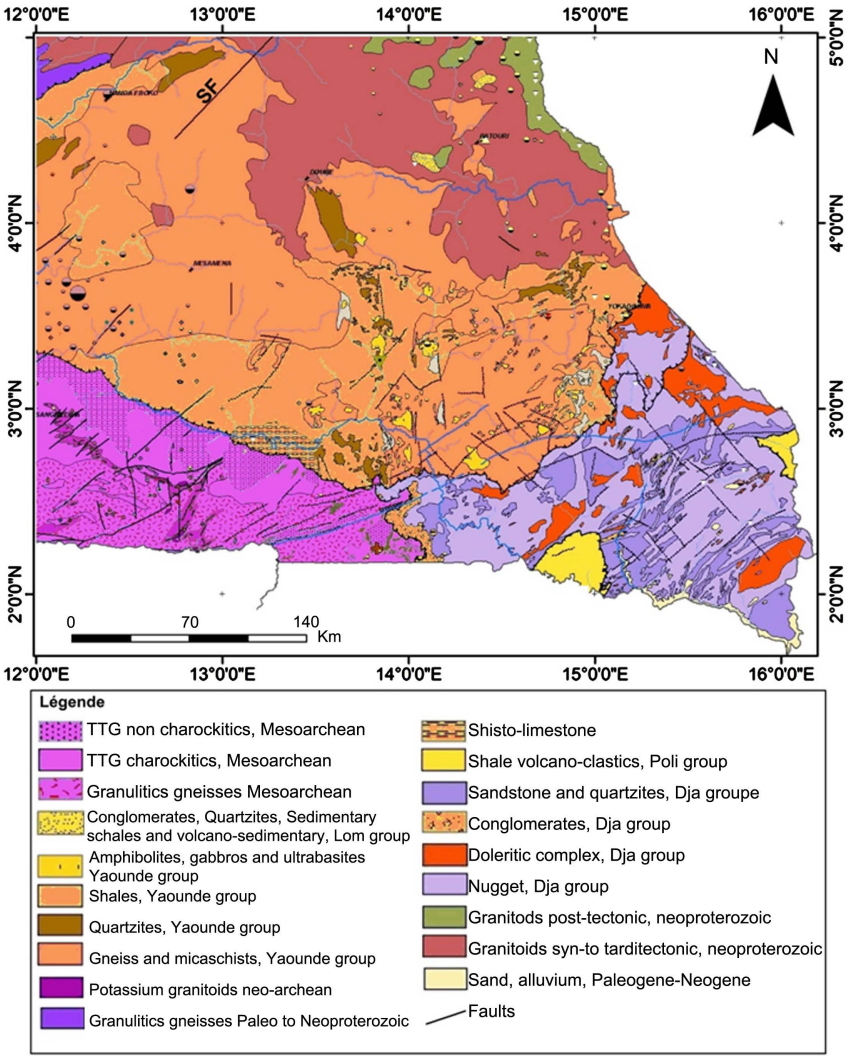

Figure 2. Geology maps of the study area [55].

The Congo Craton is one of the largest cratonic blocks in Africa with an area of about 5.7 million Km^2 with a diameter of ~2500 Km [46]. Cameroon shares with the neighbouring contries the northern edge of the largest African Craton called the Congo Craton [47]. The Ntem Complex located in the southern part of Cameroon is mainly composed by early Proterozoic syenites and constitutes the northern edge of the Archean Congo Craton domain [41] [48] [49]. It has been first influenced by the Liberian orogeny marked by various folds and brittle structures [50] with an Archaean magnetism rocks with some reworked material that formed in early Proterozoic times [51] [52] [53].

The Yaounde domain is a huge nappe thrusted southward onto the Congo Craton. It comprises low to high grade garnet bearing shale, gneisses and orthogneisses transformed under a medium to high pressure metamorphism reaching the granulite facies [39]. In the Yaounde domain, [54] showed that the tectonic caused by overall dextral transgressions due to alternating E-W to NW-SE contractions and N-S to NE-SW orogenic-parallel extensions generated N or S foliation penetration associated with ENE-WSW stretching lineation and a N-S to NE-SW folding. However, the tectonic evolution of the southern Cameroon is still debated regarding the collision system, the strike-slip direction and the history of the complexity of its geodynamics.

3. Origin of Data

The gravity data used in this work are the combination of the XGM2016 global gravitational model used to generate the free-air gravity anomaly and the ETOPO1 topographic and bathymetric datasets [56] used to compute the topographic and bathymetric gravity corrections. To get the Bouguer anomalies data, we applied these gravity corrections to the free-air gravity anomaly. The experimental Gravity Field Model XGM2016, parameterized as a spherical harmonic series up to degree and order 719, was computed as a precursor study for the upcoming combined Earth Gravitational Model 2020 (EGM2020). The combination methodoly of XGM2016 is the same as its predecessor model GOCOO5c [57]. The main difference between XGM2016 and GOCOO5c models is that XGM2016 is supported by an improved terrestrial data set of gravity anomaly area-means provided by the United States National Geospatial-Intelligence Agency (NGA). These differences result from including additional information of satellite data that contribute to the improved ground data in these regions. XGM2016 also yields a smoother Mean Dynamic Topography with significantly reduced artifacts, which has the benefit of enhanced information with respect to ocean area modelling.

4. Methodologies

Many filtering operations are necessary and should be applied on the Bouguer anomaly map to bring out the lineaments necessary to plot a geological model of the subsoil and highlighting the intrusions of igneous bodies in the study area

located in Cameroon. The separation by extension method of Bouguer anomalies is first summarized. Then the first order derivative filters followed by the horizontal gradient, the analytical signal, and the tilt angle and its horizontal gradient will be used to plot the edge contacts of the study area. Finally, we will used the Blakely and Simpson method [29] to apply the multi-scale horizontal derivative of the vertical derivative to also plot the edge geological contacts of the same study area and then compare the two methods and the corresponding structural maps.

4.1. Regional/Residual Separation

The extension method is the regional/residual separation method used here. It consists in determining of a suitable altitude for upward continuation after applied the Fourier transform, in the goal to obtain the optimum regional anomaly map for the study area by applying the Zeng method [58]. The maxima calculated at each altitude of upward continuation are then counted and plotted in **Figure 3**. The altitude where the maxima become zero corresponds to the altitude where the regional anomaly map is optimum [18] [59]. Thus the map extended to 30 Km corresponds to the regional anomalies map of the study area.

4.2. Derivative Filters

Let us consider that the total gravimetric intensity data is represented as ΔG, caused by the distribution of density sources beneath the surface. We can apply the derivative filters when the gravity fields of several sources interfere in the goal to determine the contact location of the sources [60]. This is due to the vertical derivative being able to isolate the gravity effects of individual sources better than the Bouguer anomaly because of it's no applying in the frequency domain which generally enhances data errors, depending on the signal/noise ratio [61]. The vertical derivative also has the advantage to operate the calculation at several heights using a stable operator like an upward continuation [18].

Basically, we can write horizontal and vertical first-order derivatives as:

$$\frac{\partial \Delta G}{\partial x} = \frac{\Delta G_{i+1,j} - \Delta G_{i-1,j}}{2\Delta x} \tag{1}$$

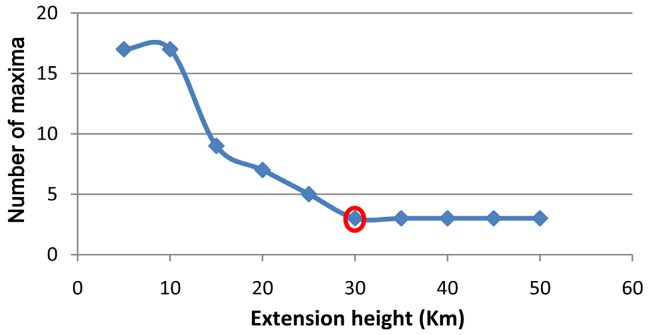

Figure 3. Number of maxima versus extension height. From h = 30 km (circle in red), the number of maxima becomes constant.

$$\frac{\partial \Delta G}{\partial y} = \frac{\Delta G_{i,j+1} - \Delta G_{i,j-1}}{2\Delta y} \tag{2}$$

$$\frac{\partial \Delta G}{\partial z} = F^{-1}\left\{|k| F\left(\Delta G\right)\right\} \tag{3}$$

where, Δx and Δy are sample intervals, i and j represent the measurements of ΔG, F and F^{-1} are defined as the Fourier transform and inverse Fourier transform and $|k|$ is the radial wavenumber.

To calculate the Horizontal Gradient Amplitude (HGA) [30] [31] and the Analytic Signal Amplitude (ASA) [32] [33] [34], we can combine these quantities as follows:

$$\text{HGA} = \sqrt{\left(\frac{\partial \Delta G}{\partial x}\right)^2 + \left(\frac{\partial \Delta G}{\partial y}\right)^2} \tag{4}$$

$$\text{ASA} = \sqrt{\left(\frac{\partial \Delta G}{\partial x}\right)^2 + \left(\frac{\partial \Delta G}{\partial y}\right)^2 + \left(\frac{\partial \Delta G}{\partial z}\right)^2} \tag{5}$$

These filters are efficient to isolate boundaries since maximum value usually is located above the source, especially when symmetry is present [62] [63].

4.3. Phase Filters

The Tilt Angle (TDR) is one of the most phase filters used today to highlight geological information. The tilt derivative and its total horizontal derivative are useful for mapping shallow basement structures and mineral exploration targets [35]. They proposed an interesting approach known as tilt angle (tilt filter). They used the ratio of the vertical derivative to the absolute amplitude of the horizontal gradient when applied to potential data in order to define the tilt angle as follows:

$$\text{TDR} = \tan^{-1}\left[\frac{\dfrac{\partial \Delta G}{\partial z}}{\sqrt{\left(\dfrac{\partial \Delta G}{\partial x}\right)^2 + \left(\dfrac{\partial \Delta G}{\partial y}\right)^2}}\right] \tag{6}$$

The horizontal gradient of tilt angle (HG_{TDR}) was developed by many researchers like [64] and [65] to improve the results of the tilt angle method. It is given by:

$$\text{HG}_{\text{TDR}} = \sqrt{\left(\frac{\partial \text{TDR}}{\partial x}\right)^2 + \left(\frac{\partial \text{TDR}}{\partial y}\right)^2} \tag{7}$$

4.4. Determination of Edge Contacts Using Phase Filters

For determination of precise edges, the TDR and HG_{TDR} are well indicated but the HG_{TDR} is more precise than the TDR because it detects very faint edges better than it. [36] shows that the TDR is a good approach to equalize disparate signals, but it is not primarily an edge detection filter because it uses its zero contours to detect the source edges. The edge of HG_{TDR} will be plotted using the Blakely and

Simpson method and then, the map of zero contours of TDR and the one of HG_{TDR} will be used to plot the corresponding structural map of the study area.

4.5. Determination of Edge Contacts Using the Multi-Scale Horizontal Derivative of Vertical Derivative Method

The upward continuation of the gravity field at increasing heights has the particularity of highlighting the gravity effect of deeper sources. To determine the geological contacts, it is important to know that the highest upward continuation corresponds to the gravity response of the deepest part of the contact. When the contact is located vertically to the source, the maxima of the total horizontal gradient of the upward continuation fields are located at the same position and when the maxima systematically shift in a horizontal direction, the dip direction of the contact should be identified [60].

That method involves the following steps:

- Calculating the first-order vertical derivative for upward continued gravity field at different heights, called here the multi-scale vertical derivative;
- Determining the maxima of the horizontal gradient of the multi-scale vertical derivative;
- Superposing the maps obtained for different continuation heights.

5. Results

5.1. Bouguer Anomaly Map

The data resulting from the combination of the XGM2016 global gravitational model and ETOPO1 topographic and bathymetric datasets were used to gridded the Bouguer anomalies map with a grid cell size of 5000 m grid space to show the spatial distribution of gravity anomaly. The corresponding map is called the Total Gravity Intensity (TGI). It clearly displays the differences in locations of high gravimetric intensities that reach the peak of −8.5 mGal and low gravimetric intensities that the lowest reached the peak of −112.4 mGal (**Figure 4**). The

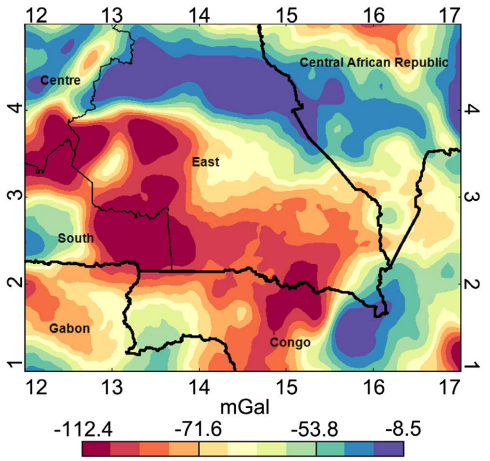

Figure 4. Bouguer anomaly map of the study area computed from the XGM2016 on a 0.1˚ × 0.1˚ geographical grid (black lines represent national and regional boundaries).

signal of this map is affected with many noises due to the effects of regional on the distribution of gravity anomalies and a direct interpretation without eliminating these effects will contain errors. To make it, we need to separate the regional effects from the Bouguer and this will be the subject of the next section.

5.2. Regional/Residual Maps

As explained previously in Section 4, the Bouguer anomalies map extended to 30 Km corresponds to the regional anomalies map (**Figure 5(a)**). Now, it we will subtract from the Bouguer anomalies map to get the corresponding residual anomalies map (**Figure 5(b)**) representing in **Figure 4** and which will be the basis of the various filtering operations that will follow.

The positive anomalies with peaks reaching 38 mGal observed on the regional anomaly map correspond to Neoproterozoic series made up of post to syn-tectonic granitoids. The average intensity anomalies observed on the residual map are mostly nuggets, sandstones and quartzites of the Dja group. The negative anomalies observed correspond to Mesoarchean gneiss and volcano-clastic sandstones of the Poli group and the conglomerates, quartzites, sedimentary sandstones and volcano-sedimentary sandstones of the Lom group. Finally, we can observe a great correlation between the residual anomalies map and the geological map of the study area. Theses anomalies would be caused by the effects of surface structures present in the study area.

5.3. Derivative Filter

The first-order derivative filters have been applied according to the procedures schematically described in section 4 in the goal to highlight the gravimetric signatures of the study area. The Z-derivative map represented in **Figure 6** presents a good distribution of the anomalies with peaks range from −2 Gal to 3 Gal. The positive anomalie observed at point A is more highlighted and could represented the volcano-clastic sandstones of the Poli group as represented on the geological map.

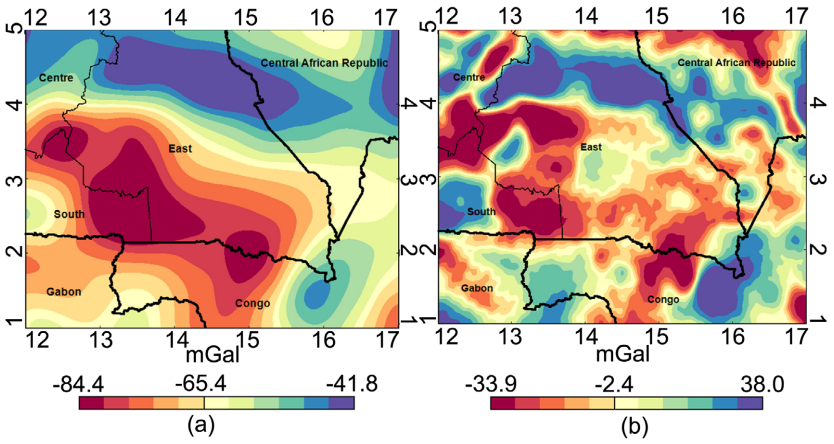

Figure 5. (a) Bouguer regional map; and (b) Bouguer residual map (black lines represent national and regional boundaries).

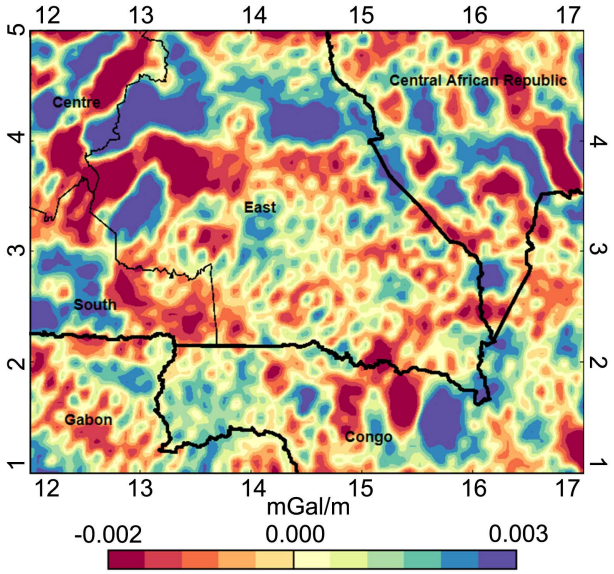

Figure 6. First order Z-derivative of Bouguer residual anomalies map (black lines represent national and regional boundaries).

5.4. Gradients Filters

The horizontal (**Figure 7(a)**) and total gradient amplitude (**Figure 7(b)**) respectively noted HGA and ASA were applied to the residual map in the goal to identify isolated sources, since in most cases the filtered anomaly is entirely positive and the maximum value is located above the source. The gradient maps represented in **Figure 7** better represented the anomalies and we can observed that the positive and negative anomalies which were grouped on the Bouguer regional map are isolated and the gradients filters aim to center the gravity anomalies below their geological sources. We can observe a less difference between these two figures in the highlighting of the positives anomalies represented at the northwest part of the study area and this can be explained by the fact that the ASA is more indicated to detect geologic sources and boundaries of the shallowest sources than the HGA, since it adds the vertical derivative in its formulation. These filters are not sufficient for a good interpretation of the anomalies observed in the study area because they are limited to a qualitative interpretation, but furthermore the information that it gives corroborate the one observe on the geological map.

5.5. Phase Filters

The phase filters are not used to determinate the locations of anomalies responsible to the body intrusions as the gradient filters, but are instead used to determinate the edges contacts such as faults. The TDR (**Figure 8(a)**) and the HG_{TDR} (**Figure 8(b)**) filters illustrated in **Figure 8** are well indicated for determination of precise edges sources but the HG_{TDR} can be more precise than the TDR because it detects very faint edges better than it. As observed in the first order Z-derivative of Bouguer residual anomalies map (**Figure 6**), we can observe that

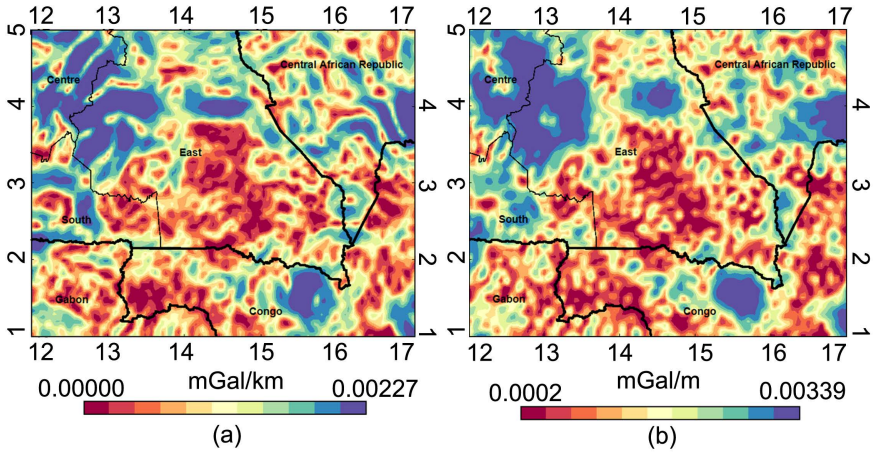

Figure 7. (a) The horizontal gradient amplitude; and (b) analytical signal amplitude of the Bouguer residual map (black lines represent national and regional boundaries).

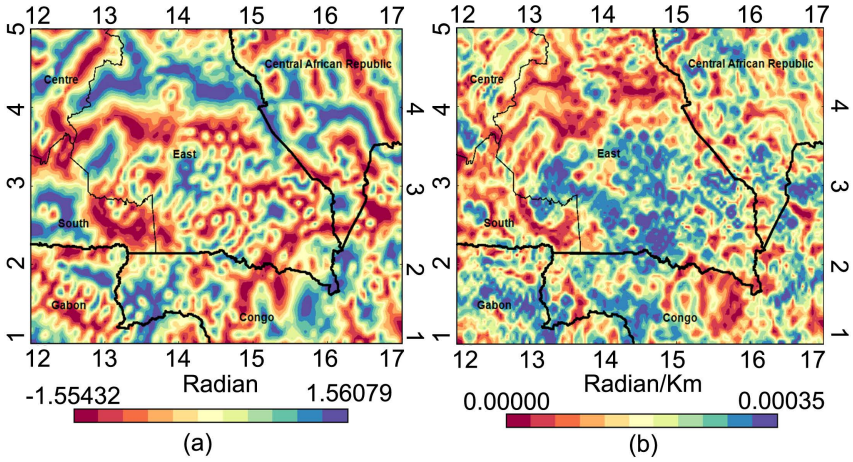

Figure 8. (a) The Tilt Angle (TDR); and (b) the horizontal gradient of tilt derivative (HG_{TDR}) of the Bouguer residual map (black lines represent national and regional boundaries).

there is a very great similarity on this one and the map of TDR, and the map of TDR would therefore represent the geological contacts at the origin of these intrusions. The HG_{TDR} map isolated contact edges both from shallow and deep structures existing below them because it is the application of a gradient filter on the TDR.

5.6. Determination of Structural Map Using Phase Filters

[36] shows that the TDR is a good approach to equalize disparate signal but, it is not primarily an edge detection filter because it uses its zero contours to detect the source edges while the HG_{TDR} use it maxima to determine the position of the source edge. The zero-contours map of the TDR (**Figure 9(a)**) and the source edges map of HG_{TDR} (**Figure 9(b)**) will be used and analyzed together to draw the structural map responsible to the fracturing in the study area, which will be represented in **Figure 10(a)**.

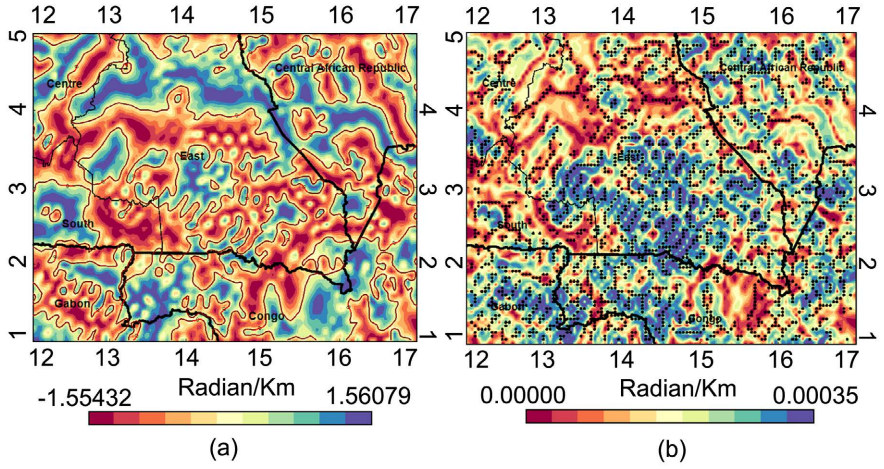

Figure 9. (a) Zero contours map of TDR; and (b) source edges map of HG_{TDR}, (black lines represent national and regional boundaries).

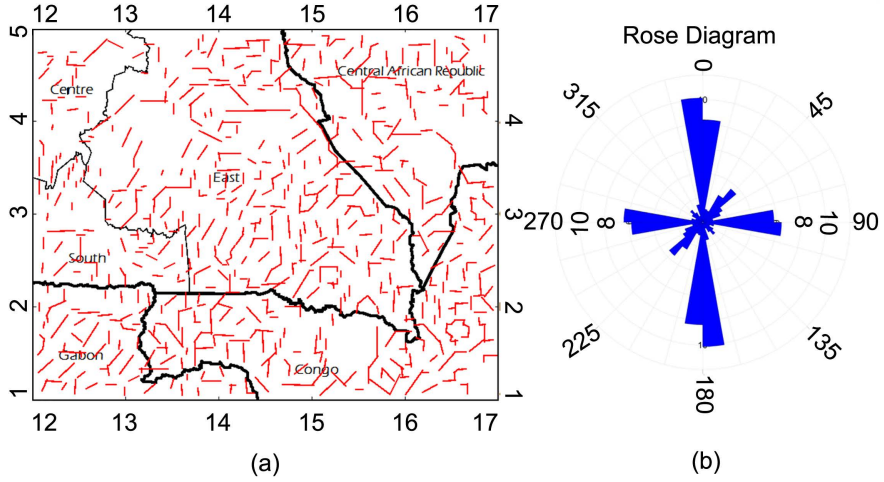

Figure 10. (a) Structural map of the study area using phase filters; and (b) rose diagram that shows the fault orientations within Southeast Cameroon,(black lines represent national and regional boundaries).

The rose diagram of the structural direction represented in the map of **Figure 10(b)** shows that the fracturing in this zone was done along 3 main directions namely N-S, W-E and SW-NE and the major direction of fracturing in southeast Cameroon is N-S.

5.7. Determination of Structural Map Using MSHDVD Method

The detailed methodology for this section has been developed in previous section 4. In this section, using the maxima method, we have identified all the edges contact successively at depths 2, 4, 6, 8 and 10 Km. The map in **Figure 11(a)** represents the contact map at different height and **Figure 11(b)** represents the corresponding structural map.

The rose diagram of the structural direction drown with MSHVDV method represented in **Figure 12** shows that the fracturing in the study area was done

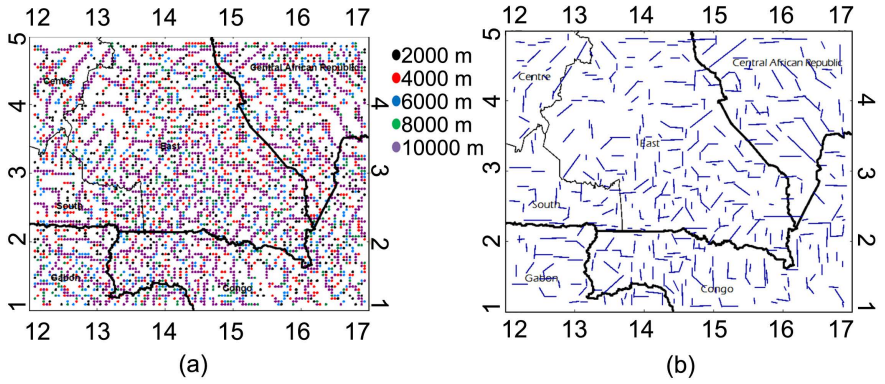

Figure 11. (a) Source edges of study area obtained by the MSHDVD method at different height; and (b) structural map of the study area using the MSHDVD method, (black lines represent national and regional boundaries).

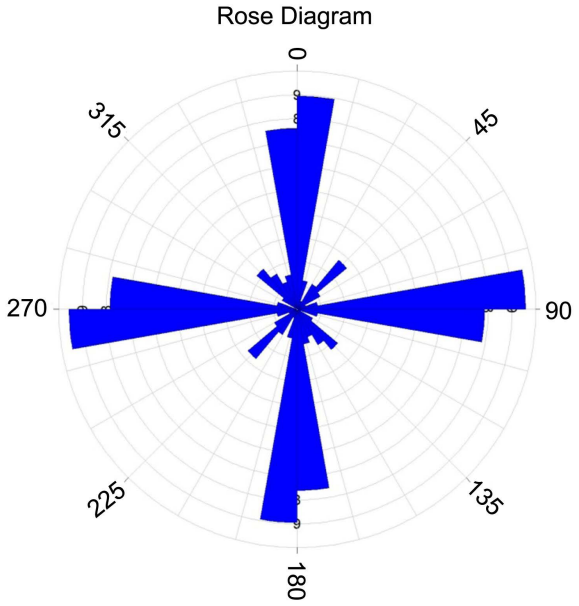

Figure 12. Rose diagram that shows the fault orientations within Southeast Cameroon according to MSHDVD method.

along 4 directions namely N-S, W-E, NW-SE SW-NE and the major direction of fracturing in southeast Cameroon according to MSHDVD methos is W-E.

6. Discussion

The Bouguer residual anomaly map (**Figure 5(b)**) highlights a large positive anomaly located at the north of the study area, a large medium anomaly located to the center to the southeast and many large negative anomalies located both at the west and the southwest. These variations observed on the lithology are due to cross cut by post-metamorphic and post deformation intrusions, both covered by discordant glacial deposits overlain by carbonate formations of the upper Dja series called Mintom Formation and the overthrusting unit including the Yoka-douma series overlapping the folded unit [66]. This map presents the distribu-

tion of anomalies more precisely than the one of Bouguer and is similar to that one. This resemblance rate to the Bouguer anomaly map justifies the chosen separation method and validates the extension height which is 30 km. finally, we can observed that the repartition of these anomalies in block can not a priori informed on the structural directions.

The first-order Z-derived map (**Figure 6**) enhances the information contained in the residual map. It dissociated the anomalies that were represented in block and shows some positive anomalies that were not visible on the residual map. The gradient maps (**Figure 7**) isolate the different sources that were arranged as a block and place the gravity anomalies directly above their sources.

The TDR map (**Figure 8(a)**) highlights the different gravimetric domains while the HG_{TDR} map (**Figure 8(b)**) highlights the different contacts that delimit these different domains. Now, we can observe the main structural directions responsible for the fracturing in the southeast of Cameroon. These directions can be WSW-ENE, W-E and NNW-SSE. The zero contours map (**Figure 9(a)**) highlights the various contacts that would be at the origin of the various anomalies while the source edge maps (**Figure 9(b)**) justify at these points the presence of the various corresponding anomalies. Thus, we believe that the structural map obtained by phase filters (**Figure 10(a)**) is better suitable for highlighting geological contacts as faults. The corresponding rose diagram (**Figure 10(b)**) shows that the main structural direction of the study area is N-S, followed by W-E and SW-NE. That information would be correct because the fracturing will follow the one of the Sanaga Fault that causes a moving of the crust from these directions.

The sources edge determined by the MSHDVD method represented in **Figure 11(a)** is not easy to interpret because it determinates the contacts at precise different depths. The structural corresponding map highlights most of the contacts shown on the structural map obtained by phase filters but the main structural directions here are W-E followed by N-S. This information corroborates the previous one, but we note that the methodology used to plot that faults were not very efficient.

Our results highlight some structures that already existed according to the observations of the geological map, but also highlight new faults.

7. Conclusions

In this research work, we separated the regional/residual anomalies by the extension method in order to obtain the best map of residual anomalies which was the result of subtraction of the Bouguer map upwards to 30 Km from the Bouguer map. Then we used filters such as HG, AS, TDR and HG_{TDR} gradient to enhance the geological information and highlight the geological source edges responsible for these anomalies. Finally, we also used the MSHDVD method to highlight the edge contacts and we observed that this method is not more precise than the first one. The main result of this work is the structural map obtained by the interpre-

tation of phase filters, with the main structural direction known as N-S. This shows the major lineaments of the region and faults of various directions with high precision. These results are comparable to those existing and corroborate the information on the geological map. Also, the large fault network plotted shows that the south-east of Cameroon would be a compression zone due to the strike-slip fault network of the Sanaga, and this fault network justifies the presence of a great mineralization activity which would have led to the formation of minerals of varied nature that exists in the southeast of Cameroon.

The geological structures observed show that the tectonic activity in this region is still ongoing. However, it would be important to delineate the depths of the structures that form the observed main structures by quantitative analysis, inversion and/or by 2D or 3D modelling. Also, the use of remote sensing data and minerals analysis will make it possible to precisely highlight the mineralogy of the said region with the goal to complete the geological information.

Acknowledgements

The authors are grateful to the editor of the journal and the two unknown reviewers for detailed and constructive reviews, which significantly improved the original manuscript. All grid files and maps were created using Oasis montaj v8.4.

Conflicts of Interest

The authors declare no conflicts of interest regarding the publication of this paper.

References

[1] Telford, W.M., Geldart, L. and Sheriff, R.E. (1990) Applied Geophysics. Cambridge University Press, Cambridge. https://doi.org/10.1017/CBO9781139167932

[2] Blakely, R.J. (1996) Potential Theory in Gravity and Magnetic Applications. Cambridge University Press, Cambridge. https://doi.org/10.1017/CBO9780511549816

[3] Skeels, D.C. (1967) What Is Residual Gravity? *Geophysics*, **32**, 872-876. https://doi.org/10.1190/1.1439896

[4] Vajda, P., Vanícek, P. and Meurers, B. (2004) On the Removal of the Effect of Topography on Gravity Disturbance in Gravity Data Inversion or Interpretation. *Contributions to Geophysics and Geodesy*, **34**, 339-369.

[5] Sjöberg, L.E., Bagherbandi, M. and Tenzer, R. (2015) On Gravity Inversion by No-Topography and Rigorous Isostatic Gravity Anomalies. *Pure and Applied Geophysics*, **172**, 2669-2680. https://doi.org/10.1007/s00024-015-1032-y

[6] Tenzer, R., Chen, W., Tsoulis, D., Bagherbandi, M., Sjoberg, L.E., Novak, P. and Jin, S. (2015) Analysis of the Refined CRUST1.0 Crustal Model and Its Gravity Field. *Surveys in Geophysics*, **36**, 139-165. https://doi.org/10.1007/s10712-014-9299-6

[7] Bai, Y., Dong, D., Kirby, J.F., Williams, S.E. and Wang, Z. (2018) The Effect of Dynamic Topography and Gravity on Lithospheric Effective Elastic Thickness Estimation: A Case Study. *Geophysical Journal International*, **214**, 623-634.

https://doi.org/10.1093/gji/ggy162

[8] Tenzer, R. and Chen, W. (2019) Mantle and Sub-Lithosphere Mantle Gravity Maps from the LITHO1.0 Global Lithospheric Model. *Earth-Science Reviews*, **194**, 38-56. https://doi.org/10.1016/j.earscirev.2019.05.001

[9] Hinze, W.J., Von Frese, R.R. and Saad, A.H. (2013) Gravity and Magnetic Exploration: Principles, Practices, and Applications. Cambridge University Press, Cambridge. https://doi.org/10.1017/CBO9780511843129

[10] Griffin, W.R. (1949) Residual Gravity in Theory and Practice. *Geophysics*, **14**, 39-56. https://doi.org/10.1190/1.1437506

[11] Henderson, R.G. and Zietz, I. (1949) The Computation of Second Vertical Derivatives of Geomagnetic Fields. *Geophysics*, **14**, 508-516. https://doi.org/10.1190/1.1437558

[12] Roy, A. (1958) Residual and Second Derivative of Gravity and Magnetic Maps. *Geophysics*, **23**, 860-862. https://doi.org/10.1190/1.1438535

[13] Agocs, W.B. (1951) Least Squares Residual Anomaly Determination. *Geophysics*, **16**, 686-696. https://doi.org/10.1190/1.1437720

[14] Zurflueh, E.G. (1967) A Fourier Method for the Regional-Residual Problem of Potential Fields. *Geophysics*, **32**, 1015-1035. https://doi.org/10.1190/1.1439905

[15] Agarwal, R.G. and Kanasewich, E.R. (1971) Automatic Trend Analysis and Interpretation of Potential Field Data. *Geophysics*, **36**, 339-348. https://doi.org/10.1190/1.1440173

[16] Syberg, F.J.R. (1972) A Fourier Method for the Regional-Residual Problem of Potential Fields. *Geophysical Prospecting*, **20**, 47-75. https://doi.org/10.1111/j.1365-2478.1972.tb00619.x

[17] Spector, A. and Grant, F.S. (1970) Statistical Models for Interpreting Aeromagnetic Data. *Geophysics*, **35**, 293-302. https://doi.org/10.1190/1.1440092

[18] Jacobsen, B.H. (1987) A Case for Upward Continuation as a Standard Separation Filter for Potential-Field Maps. *Geophysics*, **52**, 390-398. https://doi.org/10.1190/1.1442378

[19] Pawlowski, R.S. and Hansen, R.O. (1990) Gravity Anomaly Separation by Wiener Filtering. *Geophysics*, **55**, 539-548. https://doi.org/10.1190/1.1442865

[20] Pawlowski, R.S. (1995) Preferential Continuation for Potential-Field Anomaly Enhancement. *Geophysics*, **60**, 390-398. https://doi.org/10.1190/1.1443775

[21] Tadjou, J.M., Nouayou, R., Kamguia, J., Kande, H.L. and Manguelle-Dicoum, E. (2009) Gravity Analysis of the Boundary between the Congo Graton and the Pan-African Belt of Cameroon. *Austrian Journal of Earth Sciences*, **102**, 71-79.

[22] Poudjom Djomani, Y.H., Nnange, J.M., Diament, M., Ebinger, C.J. and Fairhead, J.D. (1995) Effective Elastic Thickness and Crustal Thickness Variations in West Central Africa Inferred from Gravity Data. *Journal of Geophysical Research*, **100**, 22047-22070. https://doi.org/10.1029/95JB01149

[23] Tokam, A.P.K., Tabod, C.T., Nyblade, A.A., Julia, J., Wiens, D.A. and Pasyanos, M.E. (2010) Structure of the Crust beneath Cameroon, West Africa, from the Joint Inversion of Rayleigh Wave Group Velocities and Receiver Functions. *Geophysical Journal International*, **183**, 1061-1076. https://doi.org/10.1111/j.1365-246X.2010.04776.x

[24] Shandini, Y. and Tadjou, J.M. (2012) Interpreting Gravity Anomalies in South Cameroon, Central Africa. *Earth Sciences Research Journal*, **16**, 5-9.

[25] Guidarelli, M. and Aoudia, A. (2016) Ambient Noise Tomography of the Cameroon

Volcanic Line and Northern Congo Craton: New Constraints on the Structure of the Lithosphere. *Geophysical Journal International*, **204**, 1756-1765. https://doi.org/10.1093/gji/ggv561

[26] Ngalamo, J.F.G., Sobh, M., Bisso, D., Abdelsalam, M.G., Atekwana, E. and Ekodeck, G.E. (2018) Lithospheric Structure beneath the Central Africa Orogenic Belt in Cameroon from the Analysis of Satellite Gravity and Passive Seismic Data. *Tectonophysics*, **745**, 326-337. https://doi.org/10.1016/j.tecto.2018.08.015

[27] Ghomsi, F.E.K., Severin, N., Mandal, A., Nyam, F.E.A., Tenzer, R., Kamga, A.P.T. and Nouayou, R. (2020) Cameroon's Crustal Configuration from Global Gravity and Topographic Models and Seismic Data. *Journal of African Earth Sciences*, **161**, Article ID: 103657. https://doi.org/10.1016/j.jafrearsci.2019.103657

[28] Nyaban, C.E, Ndougsa-Mbarga, T., Bikoro-Bi-Alou, M., Manekeng, S.A.T. and and Assembe, S.P. (2021) Multi-Scale Analysis and Modelling of Aeromagnetic Data over the Bétaré-Oya Area in Eastern Cameroon, for Structural Evidence Investigations. *Solid Earth*, **12**, 785-800. https://doi.org/10.5194/se-12-785-2021

[29] Blakely, R.J. and Simpson R.W. (1986) Approximating Edges of Source Bodies from Magnetic or Gravity Anomalies. *Geophysics*, **51**, 1494-1498. https://doi.org/10.1190/1.1442197

[30] Cordell, L. (1979) Gravimetric Expression of Graben Faulting in Santa Fe Country and the Espanola Basin, New Mexico. Geological Society Guidebook. In: Ingersoll, R.V., Woodward, L.A. and James, H.L., Eds., 30*th Field Conference*, New Mexico, 59-64. https://doi.org/10.56577/FFC-30.59

[31] Cordell, L. and Grauch, V.J.S. (1985) 16. Mapping Basement Magnetization Zones from Aeromagnetic Data in the San Juan Basin, New Mexico. In: Hinze, W.J., Ed., *The Utility of Regional Gravity and Magnetic Anomaly Maps*, Society of Exploration Geophysicists, Houston, 181-197. https://doi.org/10.1190/1.0931830346.ch16

[32] Nabighian, M.N. (1972) The Analytic Signal of Two-Dimensional Magnetic Bodies with Polygonal Cross-Section: Its Properties and Use for Automated Anomaly Interpretation. *Geophysics*, **37**, 507-517. https://doi.org/10.1190/1.1440276

[33] Nabighian, M.N. (1984) Toward a Three-Dimensional Automatic Interpretation of Potential Field Data via Generalized Hilbert Transforms: Fundamental Relations. *Geophysics*, **49**, 780-786. https://doi.org/10.1190/1.1441706

[34] Roest, W.R., Verhoef, J. and Pilkington, M. (1992) Magnetic Interpretation Using the 3-D Analytic Signal. *Geophysics*, **57**, 116-125. https://doi.org/10.1190/1.1443174

[35] Miller, H.G. and Singh, V. (1994) Potential Field Tilt—A New Concept for Location of Potential Field Sources. *Journal of Applied Geophysics*, **32**, 213-217. https://doi.org/10.1016/0926-9851(94)90022-1

[36] Pham, L.T., Eldosouky, A.M., Oksum, E. and Saada, S.A. (2020) A New High Resolution Filter for Source Edge Detection of Potential Field Data. *Geocarto International*, **37**, 3051-3068. https://doi.org/10.1080/10106049.2020.1849414

[37] Fitton, J.G. (1987) The Cameroon Line, West Africa: A Comparison between Oceanic and Continental Alkaline Volcanism. Alkali Igneous Rocks. Geological Society, London, Special Publications No. 30, 273-291. https://doi.org/10.1144/GSL.SP.1987.030.01.13

[38] Poudjom Djomani, Y.H., Diament, M. and Wilson, M. (1997) Lithospheric Structure across the Adamawa Plateau (Cameroon) from Gravity Studies. *Tectonophysics*, **273**, 317-327. https://doi.org/10.1016/S0040-1951(96)00280-6

[39] Toteu, S.F., Penaye, J. and Poudjom Djomani, Y. (2004) Geodynamic Evolution of

the Pan-African Belt in Central Africa with Special Reference to Cameroon. *Journal of Earth Science*, **41**, 73-85. https://doi.org/10.1139/e03-079

[40] Ngako, V. (1999) Les déformations continentales panafricaines en Afrique Centrale. Résultat d'un poinçonnement de type himalayéen. Thèse Doctorat d'État, Université de Yaoundé I, Yaoundé, 241 p.

[41] Tchameni, R., Mezger, K., Nsifa, N.E. and Pouclet, A. (2000) Neoarchaean Crustal Evolution in the Congo Craton: Evidence from K Rich Granitoids of the Ntem Complex, Southern Cameroon. *Journal of African Earth Sciences*, **30**, 133-147. https://doi.org/10.1016/S0899-5362(00)00012-9

[42] Nkoumbou, C., Barbey, P., Yonta-Ngouné, C., Paquette, J.L. and Villiéras, F. (2014) Precollisional Geodynamic Context of the Southern Margin of the Pan-African Fold Belt in Cameroon. *Journal of African Earth Sciences*, **99**, 245-260. https://doi.org/10.1016/j.jafrearsci.2013.10.002

[43] Toteu, S.F., Van Schmus, W.R. and Penaye, J. (2006) The Precambrian of Central Africa: Summary and Perspectives. *Journal of African Earth Sciences*, **44**, 7-10. https://doi.org/10.1016/j.jafrearsci.2005.12.002

[44] Van-Schmus, W.R., Oliveira, E.P., da Silva Filho, A.F., Toteu, S.F., Penaye, J. and and Guimaraes, I.P. (2008) Proterozoic Links between the Borborema Province, NE-Brazil and the Central African Fold Belt. Geological Society, London, Special Publications No. 294, 69-99. https://doi.org/10.1144/SP294.5

[45] Loose, D. and Schenk, V. (2018) 2.09 Ga Old Eclogites in the Eburnian-Transamazonian Orogen of Southern Cameroon: Significance for Paleoproterozoic Plate Tectonics. *Precambrian Research*, **304**, 1-11. https://doi.org/10.1016/j.precamres.2017.10.018

[46] Shang, C.K, Liégeois, J.P., Satir, M., Frisch, W. and Nsifa, E.N. (2010) Late Archaean High-K Granite Geochronology of the Northern Metacratonic Margin of the Archaean Congo Craton, Southern Cameroon: Evidence for Pb-Loss Due to Non-Mrtamorphic Causes. *Gondwana Research*, **18**, 237-355. https://doi.org/10.1016/j.gr.2010.02.008

[47] Baranov, A.A. and Bobrov, A.M. (2018) Crustal Structure and Properties of Archean Cratons of Gondwanaland: Similarity and Difference. *Russian Geology and Geophysics*, **59**, 512-524. https://doi.org/10.1016/j.rgg.2018.04.005

[48] Maurizot, P., Abessolo, A., Feybesse, J., Johan, J.L. and Lecomte, P. (1986) Etude et prospection minière du Sud-Ouest Cameroun. Synthèse des travaux de 1978 à 1985, Thèse de Doctorat, Université d'Orléans, Orléans, 274 p.

[49] Vicat, J.P., Léger, J.M., Nsifa, E., Piguet, P., Nzenti, J.P., Tchameni, R. and Pouclet, A. (1996) Distinction, au sein du craton congolais du sud-ouest du Cameroun, de deux épisodes doléritiques initiant les cycles orogéniques éburnéen (Paléoprotérozoïque) et panafricain (Néoprotérozoïque) Comptes Rendus de l'Académie des Sciences. Série 2. *Sciences de la terre et des planètes*, **323**, 575-582.

[50] Feybesse, J.L., Johan, V., Maurizot, P. and Abessolo, A. (1987) Evolution tectono-métamorphique libérienne et éburnéenne de la partie NW du Craton du Zaïrois (SW-Cameroun). In: Matheis, G. and Balkema, S.H., Eds., *Current Research in African Earth Sciences*, A. A. Balkema, Rotterdam, 9-13.

[51] Tchameni, R. (1997) Géochimie et géochronologie des formations de l'Archéen et du PaléoprotérozoÏque du Sud Cameroun (groupe du Ntem, Craton du Congo). Thède de Doctorat, Uiversité d'Orléans, Orléans, 395 p.

[52] Shang, C.K., Siebel, W., Satir, M., Chen, F. and Mvondo-Ondoua, J. (2004) Pb-Pb and U-Pb Systematics of TTG Rocks in the Congo Craton: Constraints on Crust Formation, Magmatism and Pan-African Lead Loss. *Bulletin of Geosciences*, **79**, 205-219.

[53] Tchameni, R., *et al.* (2010) Mineralogical Constraint for Metamorphic Conditions

in a Shear Zone Affecting the Archaean Ngoulemakong Tonolite, Congo Craton (Southern Cameroon) and Retebtivity of U-Pb SHRIMP Zircon Dates. *Journal of African Earth Sciences*, **58**, 67-80. https://doi.org/10.1016/j.jafrearsci.2010.01.009

[54] Mvondo, H., Owona, S., Ondoa, J.M. and Essono, J. (2007) Tectonic Evolution of the Yaounde Segment of the Neoproterozoic Central African Orogenic Belt in Southern Cameroon. *Canadian Journal of Earth Sciences*, **44**, 433-444. https://doi.org/10.1139/e06-107

[55] Toteu, S.F., Penaye, J., Deschamps, Y., Maldan, F., Nyama-Atibagoua, B., Bouyo-Houketchang, M., Sep-Nlomgan, J.P. and Mbola-Ndzana, S.P. (2008) Géologie et ressources minérales du Cameroun. 33*rd International Geological Congress*, Oslo, 6-14 August 2008, 1 p.

[56] Amante, C. and Eakins, B.W. (2009) ETOPO1 1 Arc-Minute Global Relief Model: Procedures, Data Sources and Analysis. NOAA, Technical Memorandum NESDIS, NGDC 24, 19 p.

[57] Fecher, T., Pail, R. and Gruber, T. (2017) GOCO05c: A New Combined Gravity Field Model Based on Full Normal Aquetions and Regionally Varying Weighting. *Surveys in Geophysics*, **38**, 571-590. https://doi.org/10.1007/s10712-016-9406-y

[58] Zeng, H. (1989) Estimation of the Degree of Polynomial Fitted to Gravity Anomalies and Its Applications. *Geophysical Prospecting*, **37**, 959-973. https://doi.org/10.1111/j.1365-2478.1989.tb02242.x

[59] Abate, J.M.E., Njandjock, N.P., Ngatchou, H.E., Oyoa, V., Tabod, C.T. and Manguelle-Dicoum, E. (2016) Structure of the Crust beneath the South Western Cameroon, from Gravity Data Analysis. *International Journal of Geosciences*, **7**, 991-1008. https://doi.org/10.4236/ijg.2016.78075

[60] Fedi, M. and Florio, G. (2001) Detection of Potential Fields Source Boundaries by Enhanced Horizontal Derivative Method. *Geophysical Prospecting*, **49**, 40-58. https://doi.org/10.1046/j.1365-2478.2001.00235.x

[61] Gunn, P.J. (1975) Linear Transformation of Gravity and Magnetic Fields. *Geophysical Prospecting*, **23**, 300-312. https://doi.org/10.1111/j.1365-2478.1975.tb01530.x

[62] Grauch, V.J.S. and Cordell, L. (1987) Limitations of Determining Density or Magnetic Boundaries from the Horizontal Gradient of Gravity or Pseudogravity Data. *Geophysics*, **52**, 118-121. https://doi.org/10.1190/1.1442236

[63] Phillips, J.D. (2000) Locating Magnetic Contacts: A Comparison of the Horizontal Gradient, Analytic Signal, and Local Wavenumber Methods. In: *The SEG Technical Program Expanded Abstracts* 2000, Society of Exploration Geophysicists, Calagry, 24-84. https://doi.org/10.1190/1.1816078

[64] Verduzco, B., Fairhead, J.D., Green, C.M. and MacKenzie, C. (2004) New Insights into Magnetic Derivatives for Structural Mapping. *The Leading Edge*, **23**, 116-119. https://doi.org/10.1190/1.1651454

[65] Thurston, J.B. and Smith, R.S. (1997) Automatic Conversion on Magnetic Data to Depth, Dip and Susceptibility Contrast Using the SPITM Method. *Geophysics*, **62**, 807-813. https://doi.org/10.1190/1.1444190

[66] Caron, V., Ekomane, E., Mahieux, G., Moussango, P. and Ndjeng, E. (2010) The Mintom Formation (New): Sedimentology and Geochemistry of a Neoproterozoic, Paralic Succession in South-East Cameroon. *Journal of African Earth Sciences*, **57**, 367-385. https://doi.org/10.1016/j.jafrearsci.2009.11.006